Version 24

Metastable Crystalline AuGe Catalysts Formed During Isothermal Germanium Nanowire Growth

A. D. Gamalski[1,†], J. Tersoff[2,§], R. Sharma[3], C. Ducati[4], S. Hofmann[1]

[1]Department of Engineering, University of Cambridge, Cambridge CB3 0FA, UK

[2]IBM T. J. Watson Research Center, Yorktown Heights, NY 10598

[3]Center for Nanoscale Science and Technology, National Institute of Standards and Technology, 1000 Bureau Dr., Gaithersburg MD 20899-6203.

[4]Department of Materials Science and Metallurgy, University of Cambridge, Cambridge CB2 3QZ, UK

We observe the formation of metastable AuGe phases without quenching, during strictly isothermal nucleation and growth of Ge nanowires, using video-rate lattice-resolved environmental transmission electron microscopy. We explain the unexpected formation of these phases through a novel pathway involving large and abrupt variations in composition rather than temperature. The metastable catalyst has important implications for nanowire growth; and more broadly, the isothermal process provides both a new approach to growing and studying metastable phases, and a new perspective on their formation.

[†]adg40@cam.ac.uk, [§]tersoff@us.ibm.com

Rapid thermal quenching has long been known to produce metastable phases [1]. Understanding and controlling the nucleation of such phases is crucial to a wide range of materials, from high-performance steels [2] to pharmaceuticals [3]. Here we report a new pathway to the formation of metastable phases, radically different from conventional thermal quenching. We focus on the Au-catalyzed growth of Ge nanowires (NWs) as a model nanoscale system. Video-rate lattice-resolved environmental transmission electron microscopy (ETEM) allows us to directly observe the formation of metastable AuGe phases under strictly isothermal conditions, the opposite limit from thermal quenching. Both hexagonal closed packed (HCP) and body centered tetragonal (BCT) phases of AuGe are observed. We propose that these metastable phases occur due to abrupt variations in composition during NW growth, and that the necessary conditions for metastable AuGe formation occur naturally during the NW growth process and reflect the large deviations from equilibrium achievable in nanoscale systems. We speculate that the high Ge solubility in these metastable AuGe crystalline phases [4-8] facilitates stable vapor-solid-solid (VSS) NW growth.

Figure 1 shows catalyst particles at the tip of Ge NWs growing at temperatures between 220 °C and 270 °C in Hediluted digermane (Ge_2H_6). The images are part of video sequences [9] recorded in bright field imaging conditions at 9 frames s^{-1} by a modified Tecnai F20 ETEM [10] operated at 200 kV with a differential pumping system and a digital video camera. Temperatures are measured by a thermocouple on the TEM holder mini-furnace. The electron dose was typical for high resolution imaging, and the electron beam was never focused onto the specimen in order to minimize the effects of electron-beam-induced damage/gas dissociation [11] and modification of the specimen. The Au catalyst was prepared by thermal evaporation (nominal Au thickness < 2 nm) onto perforated SiO_2 membranes or onto 2000 mesh Cu TEM grids coated with a holey carbon film and a ~30 nm sputtered SiO_x layer. The samples were transferred in air to the ETEM.

Prior to Ge_2H_6 exposure, the Au catalyst particles are crystalline with a face centered cubic (FCC) structure. Upon Ge_2H_6 exposure, the FCC Au nanoparticles transform into a AuGe eutectic liquid, even for isothermal growth at temperatures far below the AuGe eutectic (361 °C) [12]. Upon Ge crystal nucleation and growth, the catalyst can remain liquid for seconds or minutes at the temperatures studied here. Eventually it solidifies and, as shown in Fig. 1, the

system reaches a steady state where both catalyst and NW are in the solid phase, i.e. VSS growth.

The lattice resolved ETEM data allows us to assign the crystal structures occurring during the entire process, in particular during VSS growth. Fig. 1D, F show the fast Fourier transforms (FFT) of the solid catalyst particles in Fig. 1C, E respectively. For the FFT assignment we use published unit cell parameters [6, 13, 14] and calculate their theoretical electron diffraction spot patterns. The different crystal structures and cell parameters which best fit the FFTs are summarized in Table 1.

Crystal Structure	***a* (nm)**	***b* (nm)**	***c* (nm)**
FCC Au, *Fm$\bar{3}$m*	0.408	0.408	0.408
BCT γ-AuGe, *I4/mmm*	0.340	0.340	0.286
HCP β-AuGe, *P6$_3$/mmc*	0.289	0.289	0.474

Table 1: FCC Au, HCP β-AuGe [6], and BCT γ-AuGe [13, 14] unit cells used in this study.

Fig. 1D shows the FFT of the catalyst particle in the high resolution image, Fig. 1C. We find that the FFT is best matched to the known metastable HCP phase, denoted β, viewed down the $[01\bar{1}0]^{(I)}_{HCP}$ axis. Note that the superscript "(I)" indicates the imaging axis. Table 2 shows there is good agreement between the theoretical HCP unit cell and measured angles between reflections in Fig. 1D. The closest possible match with FCC Au is viewed down $[101]^{(I)}_{FCC}$, and the angles between its reflections do not agree with the measured values, Table 2. In addition to this, by comparing the ratios between reciprocal distances (measurements given in Table 3) we find that the measured FFT deviates from the calculated β phase FFT by less than 2%.

FFT	**Crystal Structure and Imaging Axis**	**Family of Reflections**	**Calculated Angles between Reflections**	**Measured Angles between Reflections**
Fig. 1D	HCP β-AuGe; $[01\bar{1}0]^{(I)}_{HCP}$	$\{\bar{1}01\bar{1}\}/\{\bar{1}011\}$	55.6°	56.7° ± 2.0°
		$\{0002\}/\{10\bar{1}1\}$	62.2°	62.1° ± 2.0°
Fig. 1F	BCT γ-AuGe; $[\bar{1}\bar{1}1]^{(I)}_{BCT}$	$\{101\}/\{011\}$	54.1°	52.1° ± 2.0°
		$\{1\bar{1}0\}/\{101\}$	63.0°	64.1° ± 2.0°
-	FCC Au; $[101]^{(I)}_{FCC}$	$\{020\}/\{11\bar{1}\}$	54.7°	-
		$\{1\bar{1}\bar{1}\}/\{11\bar{1}\}$	70.5°	-

Table 2: The predicted and measured angles between the FFT reflections in Fig. 1D and Fig. 1F. Note that the measured angle from the FFT is an average over angles between reflections with common symmetry.

Fig. 1F shows the FFT of the catalyst particle imaged in Fig. 1E. We find that the spot pattern in Fig. 1F is best fitted to BCT phase, denoted γ, viewed down the $[\bar{1}\bar{1}1]^{(I)}_{BCT}$ axis. Table 2 shows the angles between reflections for the theoretical BCT unit cell are in good agreement

with the measured reflection angles in Fig. 1F. In contrast, from Table 2 we can rule out FCC – the closest match for FCC Au is viewed down $[101]^{(I)}_{FCC}$ which has angles radically different from the measured values. Again, by comparing the ratios between the reciprocal distances (measurements given in Table 3) we find the measured FFT deviates from the calculated γ phase FFT by less than 4%.

Crystal Structure and Corresponding FFT	Measured d-spacings (Å)	Calculated d-spacings (Å)	Family of Reflections
HCP β-AuGe; Fig. 1D	2.2	2.210	$\{10\bar{1}1\}$
	2.3	2.369	{0002}
	2.2	2.210	$\{\bar{1}011\}$
BCT γ-AuGe; Fig. 1F	2.0	2.188	{011}
	2.3	2.407	$\{1\bar{1}0\}$
	2.1	2.188	{101}

Table 3: d-spacing measurements from the FFTs in Fig.1D and Fig.1F along with the d-spacings calculated from the unit cell parameters in Table 1. Note that d-spacings were measured in the FFTs in pixels and converted into reciprocal pixels for this table. The ratios (not the absolute distances using the microscope's calibration) between the d-spacings were compared to establish assignments to the β and γ structures.

In total we analyzed the FFTs of 17 lattice resolved catalyst particles. We identified 4 catalyst particles that correspond to γ, 8 cases of β, 4 which are either γ or β, and only 1 case of FCC Au, the equilibrium crystal structure. Of these 17 particles, 14 were imaged before cooling the sample to room temperature and removing it from the ETEM. During gas exposure and growth we observed 2 cases of γ, 4 cases of β, and 2 cases that are either β or γ. In other observations after turning off the source gas, but still in vacuum at the growth temperature, we observed 1 case of γ, 2 cases of β, 1 FCC Au, and 2 cases that were either γ or β. The remaining 1 case of γ and 2 cases of β were identified with *ex situ* high resolution TEM ≈2 years after the initial NW growth experiment, indicating that these metastable phases are very long-lived at room temperature.

The β and γ phases of AuGe are previously known to form by quenching liquid AuGe alloys [5, 8, 15, 16]. Metastable phases have also been observed after cooling of Ge NW catalysts [17-19], and attributed very reasonably to the rapid cooling of these nanoscale structures, or the suppression of diffusion at such low temperatures. Thus it is quite surprising to find them forming at constant temperature, and moreover at a temperature high enough to sustain growth. One possible explanation would be if diffusion is too slow to allow separation of the liquid into Ge and Au phases, so that instead the liquid freezes into a crystal of the same

composition [1, 20-22]. This is appealing, and consistent with the fact that the metastable crystal phases occur over a broad composition range [4]. However, as the catalyst solidifies into the metastable crystalline phase we observe rapid advancement of the interface with the Ge crystallite [23]. This indicates that formation of the γ and β phases involves considerable diffusive redistribution of Ge, arguing against the occurrence of a diffusionless transformation.

Here we propose a possible formation mechanism which is novel, but consistent with the known thermodynamics and kinetics of the Au-Ge system. We begin with the calculated [24-26] equilibrium Au-Ge phase diagram, Fig. 2. The red Au liquidus line is extended to show the boundary for equilibrium between Au and the metastable liquid below the eutectic. The metastable γ and β phases exist over a range of composition [4, 5, 8]. Since there is no detailed thermodynamic data, we take a crude but reasonable model for the free energy function $g_m(x,T)$:

$$g_m(x,T) = g_0(x,T) + h_{\mathrm{mix}}(x) - s_{\mathrm{mix}}(x)T \qquad \text{Eq. 1}$$

This is the classic "regular solution" model [27], where x is the mole fraction of Ge in the $Au_{1-x}Ge_x$ alloy, T is temperature, $g_0(x,T) = (1-x)g^{\mathrm{Au}}(T) + xg^{\mathrm{Ge}}(T)$ is the free energy for unmixed Au and Ge in an HCP structure [24-26], $s_{\mathrm{mix}}(x) = -k_{\mathrm{B}}[(1-x)\ln(1-x)+x\ln(x)]$ is the molar entropy of mixing, and k_{B} is the Boltzmann constant. The mixing enthalpy is $h_{\mathrm{mix}}(x) = Cx(1-x)$, where the value $C = -12.5$ kJ mol^{-1} is chosen to give a plausible phase boundary for the present discussion (we expect that the liquidus curve for the γ phase will be similar to the β liquidus, so we do not distinguish between these here).

With Eq. (1), we can include on the phase diagram (Fig. 2) the calculated liquidus for the metastable AuGe phase. This is shown as an additional green dashed curve, calculated by the common tangent construction [2]. Although crude, the model illustrates two key properties that are important for understanding this system's behavior. The first is that the metastable liquidus curve has a smaller slope than the FCC Au liquidus. This occurs automatically for any reasonable value of C, reflecting the higher Ge composition of the metastable phase. The second is that the intersection of the stable and metastable liquidus curves must lie below the eutectic point. We know this on physical grounds – otherwise the phase would occur in equilibrium – and it provides a constraint on the possible range of C.

Next we consider the system trajectory on the phase diagram during growth. The AuGe liquid can form at temperature far below the equilibrium eutectic [12]. Then, due to the large barrier to nucleate solid Ge, during the growth process the liquid can become so highly

supersaturated with Ge that nucleation of FCC Au is thermodynamically forbidden, despite the low T [28]. This corresponds to compositions to the right of the Au liquidus (including its extension into the metastable regime, shown dotted in Fig. 2). When solid Ge finally nucleates, the Ge particle grows rapidly due to the high supersaturation, and the liquid composition drops correspondingly, as suggested by the horizontal arrows from points *a* and *b* in Fig. 2. Once the composition crosses the Au liquidus, it becomes possible for FCC Au to nucleate. Similarly, the crystalline metastable AuGe phase can nucleate once the liquid composition crosses the dashed green line in Fig. 2.

The low-T regime, below the point where the two liquidus curves cross, is particularly interesting. For the case labeled "*a*" in Fig. 2, there is a range of compositions $x_s^a < x < x_m^a$ where metastable AuGe can nucleate, but FCC Au cannot. Even if the system evolves slowly, the thermodynamics would dictate the formation of a metastable AuGe catalyst particle. Therefore, we might expect that below T_i all of the liquid AuGe particles will transform into solid metastable AuGe catalysts. If so, subsequent decomposition of the AuGe into FCC Au and Ge would require nucleation of FCC Au in the solid AuGe, and subsequent diffusion of material through solid AuGe, which will be extremely slow compared to diffusion through the liquid.

In the case labeled "*b*" thermodynamics favors formation of a FCC structure after the composition of the liquid passes though the FCC liquidus line, while nucleation of the metastable phase is still not possible in the range $x_m^b < x < x_s^b$. Nevertheless it may be possible to form a solid metastable AuGe catalyst in this temperature range. We expect that the interfacial energy between the metastable AuGe solid and the liquid is lower than between FCC Au and the AuGe liquid, since the former involves a much smaller discontinuity in composition. If so, solid AuGe may nucleate more readily than FCC Au. In process *b* (Fig. 2), if a large nucleation barrier prevents formation of FCC Au before the system passes the metastable liquidus line at x_m^b, the lower interfacial energy of metastable AuGe could cause this phase to nucleate first.

Metastable AuGe phase formation by rapid compositional variations during NW growth has intriguing similarities to thermal quenching. Just as we could expect different behavior at fixed T above or below the liquidus crossing point T_i, for quenching we could expect correspondingly different behavior for liquid composition to the left or right of this point, respectively. However, there are also important differences. Quenching of macroscopic systems typically gives a mixed-phase solid. In contrast, very rapid composition variation may be limited

to nanoscale systems, where a pure single phase is virtually guaranteed. Also, rapid composition variation occurs naturally during the isothermal NW growth process, while rapid temperature variation would require disrupting the growth process.

The different kinetic pathways observed here are schematically illustrated in Fig. 3, with the various system states labeled (*i*-*vi*). States *i* – *iii* represent the transformation of the solid Au catalyst particle into AuGe liquid during Ge_2H_6 gas exposure. The metastable liquid becomes increasingly Ge-rich until a Ge crystal seed nucleates, state *iv*. After nucleation, a brief period of solid Ge growth by the VLS mechanism occurs. The liquid catalyst particle can solidify into a metastable or stable phase, state *v* or *vi*. The thermodynamically favored endpoint is *vi*, formation of FCC Au. Yet we almost never see this. Rather, we see the transition from *iv* to *v*; and much of the discussion above has focused on explaining this unexpected behavior.

In conclusion, we have observed formation of solid AuGe metastable phases during isothermal Ge NW growth, and have proposed a mechanism to explain this. This process illustrates the striking new behavior that can occur in nanoscale systems, where very large supersaturations are readily achieved, opening kinetic pathways for solidification generally unavailable in the bulk. The small size also results in a single crystal, facilitating characterization, and minimizes extrinsic effects. We therefore believe that NWs and similar systems will provide a fruitful arena for the study of nonequilibrium phases.

Acknowledgements:

A. D. G. acknowledges funding from the Marshall Aid Commemoration Commission and the National Science Foundation. S. H. and C. D. acknowledge funding from the Royal Society. S. H. acknowledges funding from ERC grant InsituNANO (n°279342). We gratefully acknowledge the use of facilities within the LeRoy Eyring Center for Solid State Science at Arizona State University.

References:

[1] D. M. Herlach, P. K. Galenko, and D. Holland-Moritz, *Metastable Solids from Undercooled Melts* (Elsevier, Amsterdam, 2007).

[2] D. A. Porter, K. E. Easterling, and M. Y. Sherif, *Phase Transformations in Metals and Alloys* (CRC Press, Boca Raton, FL, 2009).

[3] N. Rodríguez-hornedo, and D. Murphy, J. Pharm. Sci. **88**, 651 (1999).

[4] H. Okamoto, and T. B. Massalski, Bull. Alloy Phase Diagrams **5**, 9 (1984).

[5] T. R. Anantharaman, H. L. Luo, and W. Element, Nature **210**, 1040 (1966).

[6] B. X. Liu, and M. A. Nicolet, Phys. Status Solidi A **70**, 671 (1982).

[7] A. Kikitsu *et al.*, Jpn. J. Appl. Phys. **28**, 1257 (1989).

[8] M. G. Scott, Mater. Sci. Eng. **18**, 279 (1975).

[9] See EPAPS Document No. [XXX] for a bright field ETEM video (7.5 fps, corresponding to Fig. 1C) of a Ge NW growing at 270 °C in 0.27 Pa Ge_2H_6 (30% in He) from a solid HCP β-AuGe catalyst particle. The frame rate and resolution were reduced during file size compression. The play time, however, still corresponds to original growth time. For more information on EPAPS, see http://www.aip.org/pubservs/epaps.html.

[10] Disclaimer: The full description of the procedures used in this paper requires the identification of certain commercial products and their suppliers. The inclusion of such information should in no way be construed as indicating that such products or suppliers are endorsed by NIST or are recommended by NIST or that they are necessarily the best materials, instruments, software or suppliers for the purposes described.

[11] I. Utke, P. Hoffmann, and J. Melngailis, J. Vac. Sci. Technol., B **26**, 1197 (2008).

[12] A. D. Gamalski *et al.*, Nano Lett. **10**, 2972 (2010).

[13] J. Diao, K. Gall, and M. L. Dunn, Nat. Mater. **2**, 656 (2003).

[14] M. Durandurdu, Phys. Rev. B **76**, 024102 (2007).

[15] G. Kopmann, and H. P. Nicolai, Z. Metallkd. **76**, 613 (1985).

[16] G. Schluckebier, and B. Predel, Z. Metallkd. **71**, 605 (1980).

[17] A. F. Marshall *et al.*, Nano Lett. **10**, 3302 (2010).

[18] E. Sutter, and P. Sutter, Nanotechnology **22**, 295605 (2011).

[19] T. I. Kamins, X. Li, and R. S. Williams, Nano Lett. **4**, 503 (2004).

[20] H. Jones, Rep. Prog. Phys. **36**, 1425 (1973).

[21] P. K. Galenko, and D. M. Herlach, Phys. Rev. Lett. **96**, 150602 (2006).

[22] P. Galenko, Phys. Rev. E **76**, 031606 (2007).

[23] See EPAPS Document No. [XXX] for a bright field ETEM image sequence showing the rapid nucleation and subsequent solidification of liquid AuGe particles into metastable AuGe catalysts at 255 °C in 0.67 Pa pure Ge_2H_6. For more information on EPAPS, see http://www.aip.org/pubservs/epaps.html.

[24] P. Y. Chevalier, Thermochim. Acta. **141**, 217 (1989).

[25] A. Almazouzi *et al.*, J. Appl. Phys. **70**, 1345 (1991).

[26] A. T. Dinsdale, Calphad **15**, 317 (1991).

[27] J. M. Howe, *Interfaces in Materials* (John Wiley & Sons, Inc., New York, 1997).

[28] S. Kodambaka *et al.*, Science **316**, 729 (2007).

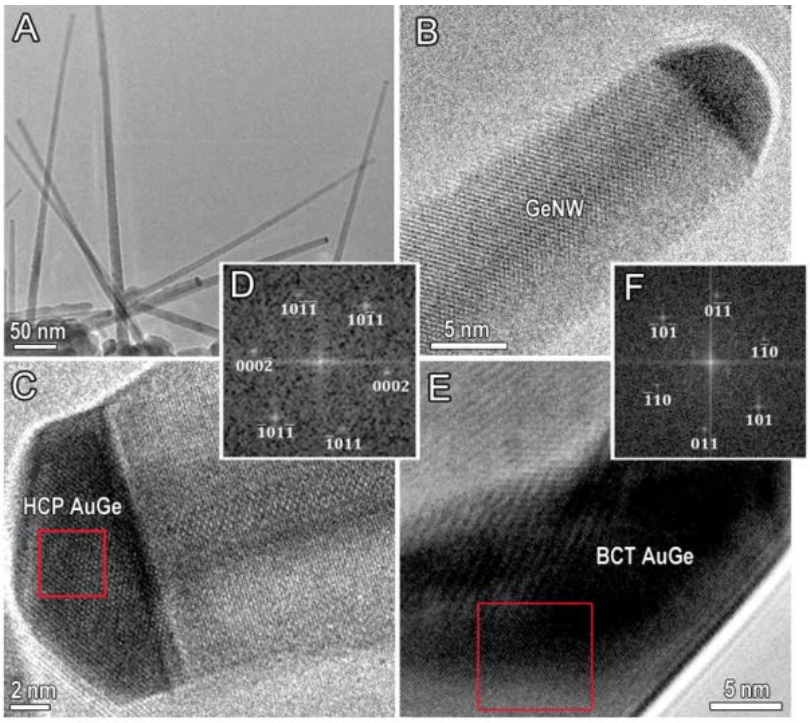

Figure 1: Various high and low magnification bright field ETEM micrographs of Ge NWs growing from solid AuGe catalysts growing in (A) $6.0 \cdot 10^{-1}$ Pa pure Ge_2H_6 at 273 °C, (B) $5.3 \cdot 10^{-2}$ Pa Ge_2H_6 (30% in He) at 272 °C, (C) $2.7 \cdot 10^{-1}$ Pa Ge_2H_6 (30% in He) at 270 °C, and (E) $6.8 \cdot 10^{-1}$ Pa Ge_2H_6 (30% in He) at 224 °C. (D) Selected area FFT of the red boxed region of the catalyst particle in (C) which matches HCP β-AuGe viewed down the $[01\bar{1}0]^{(I)}_{HCP}$ axis. (F) Selected area FFT of the red boxed region of the catalyst particle in (E) which matches the spot pattern of BCT γ-AuGe viewed down the $[\bar{1}\bar{1}1]^{(I)}_{BCT}$ axis.

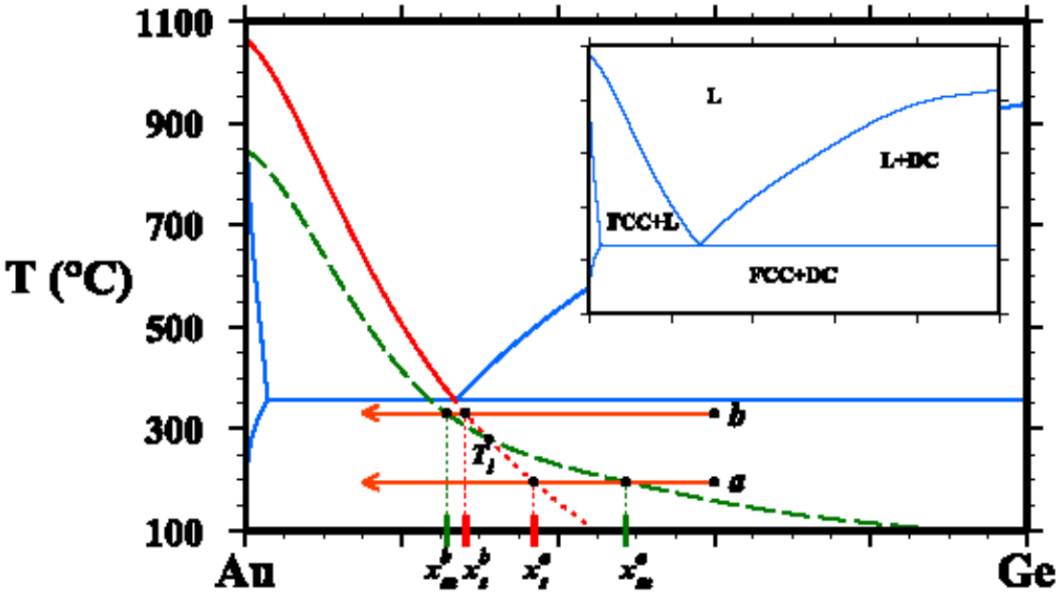

Figure 2: Calculated [24-26] phase diagram for the Au-Ge system with the metastable AuGe liquidus curve. The solidus curves, DC liquidus curve, and eutectic temperature are given in blue. The red solid curve indicates the FCC Au liquidus line above the eutectic temperature with the extended subeutectic FCC Au liquidus indicated by the dotted red curve. The green broken line indicates the metastable AuGe liquidus. The temperature where the two liquidus lines intersect is indicated by T_i. The inset is the unaltered equilibrium Au-Ge phase diagram.

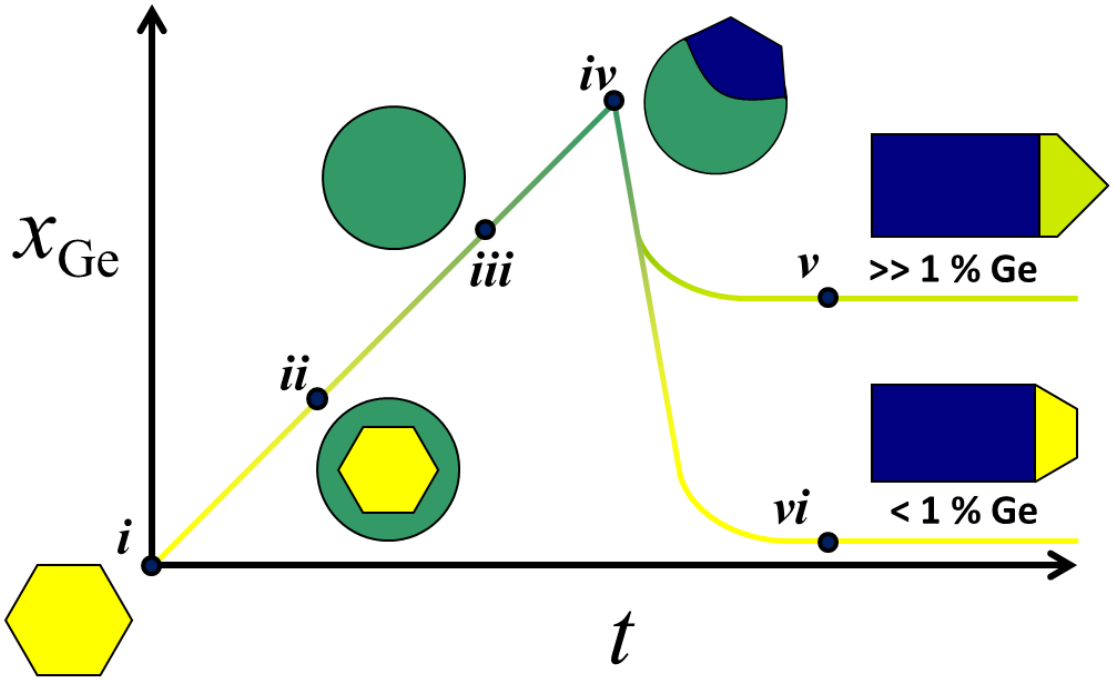

Figure 3: A schematic plot illustrating the observed Au-Ge catalyst states plotted against Ge composition in the catalyst x_{Ge} and time t (not drawn to scale). Yellow faceted shapes indicate FCC Au, solid Ge in given in blue, and metastable AuGe given by the green faceted solid. Liquid AuGe is indicated by the teal circles. From quenching experiments we expect that the metastable AuGe solid (state *v*) has composition ~15-50% Ge, while FCC Au has below 1% dissolved Ge [4-8].